

**Study of Broad Scale Anisotropy of Cosmic Ray  
Arrival Directions from  $2 \times 10^{17}eV$   
to  $10^{20}eV$  from Fly's Eye Data**

D.J. Bird<sup>1</sup>

Department of Physics, University of Illinois at Urbana-Champaign, Urbana, IL 61801,  
USA

and

H.Y. Dai<sup>2</sup>, B.R. Dawson<sup>3</sup>, J.W. Elbert, M.A. Huang<sup>4</sup>, D.B. Kieda, S. Ko, E.C. Loh, M.  
Luo<sup>5</sup>, J.D. Smith, P. Sokolsky, P. Sommers, S.B. Thomas  
Department of Physics, University of Utah, Salt Lake City, UT 84112, USA

**ABSTRACT**

We report results on the broad scale anisotropy of cosmic ray arrival directions in the energy range from  $2 \times 10^{17}eV$  to  $10^{20}eV$ . The data was taken by the Fly's Eye detector in both monocular and stereo modes of operation. We look for dependence on galactic latitude or supergalactic latitude by fitting the data to a Wdowczyk and Wolfendale plane enhancement function and a N-S gradient functional form. We report a small but statistically significant galactic plane enhancement in the energy range between  $2 \times 10^{17}eV$  and  $3.2 \times 10^{18}eV$ . The probability that this anisotropy is due to fluctuations of an isotropic distribution is less than 0.06%. The most significant galactic plane enhancement factor  $f_E = 0.104 \pm 0.036$  is in the energy range  $0.4 - 1.0 \times 10^{18}eV$ . No statistically significant evidence for a N-S gradient is found. There is no sign of significant deviation from isotropic background when the data is analyzed in terms of supergalactic latitude distributions.

---

<sup>1</sup>present address:Defence Science and Technology Organisation, P.O Box 1500, Salisbury, S.A. 5108, Australia, Australia

<sup>2</sup>present address:Rosetta Inpharmatics, 12040 115th Ave NE, Kirkland, WA 98034, USA

<sup>3</sup>present address:Department of Physics and Mathematical Physics, University of Adelaide, Adelaide, South Australia 5005, Australia

<sup>4</sup>present address:Institute of Physics, Academia Sinica, 11529 Nankong, Taiwan, ROC

<sup>5</sup>present address:Biology Division, Dugway Proving Ground, UT 84002, USA

*Subject headings:* Cosmic rays — Galaxy: general — Large-scale structure of universe

## 1. Introduction

There have been a number of reports (Gillerman & Watson 1993, Stanev et al., 1995) of small anisotropies in the ultra high energy cosmic ray arrival direction distribution with respect to the galactic or supergalactic plane. Recently, a high statistics search for anisotropy has been reported by the Akeno/AGASA collaboration (Hayashida et al. 1998). This group reports a small anisotropy towards the galactic plane at energies near  $10^{18}eV$ . The statistical significance of this evidence is not strong, however, and the various ground array experiments have reported systematic errors due to temperature and pressure variations and detector energy scale estimation which are quite different from the systematic errors in Fly’s Eye type of experiments. It is therefore important, both from the point of view of statistics and systematics, to have as complete a picture as possible of all the evidence on anisotropy. This paper is the final result on cosmic ray anisotropy from the original Fly’s Eye experiment (Baltrusaitis et al. 1985, Cassiday 1985) which ran from 1981 to 1992. Previous publications (Bird et al. 1993a, Bird et al. 1993c) were based on subsets of this complete data sample.

Observation of cosmic ray anisotropy, when taken together with studies of the cosmic ray spectral shape and cosmic ray composition can yield very important clues to the nature of the highest energy cosmic rays. If cosmic rays come from the galactic plane and are largely protonic in composition, we expect to see a galactic plane enhancement which becomes more significant with energy, since the proton rigidity will increase. A heavy composition dominated by Iron nuclei will tend to show much smaller anisotropy at any given energy because of the smaller Larmor radius of the heavy nuclei. Previously reported Fly’s Eye data on spectrum (Bird et al. 1994) and composition (Bird et al. 1993b, Bird et al., 1993d) support a two component model where a mostly heavy galactic composition is superceded by a mostly light, extragalactic component. The cross-over between these two cosmic ray fluxes appears to be near  $3 \times 10^{18}eV$ . If correct, this model would imply at best a small galactic plane enhancement below  $3 \times 10^{18}eV$ .

If the higher energy cosmic ray flux is indeed mostly extragalactic, it may have a different anisotropy from the lower energy component. Strong nearby extragalactic sources could lead to strong anisotropies at energies near  $10^{20}eV$ . If extragalactic magnetic fields

are not greater than a nanogauss (Kronberg 1994), charged particle astronomy becomes possible at these energies. It has been recently suggested that extragalactic sources may be distributed along the supergalactic plane (Stanev et al., 1995). If so, we might expect an enhancement of cosmic ray arrival directions towards this plane at high enough energies. Of course, extragalactic sources might have a more complex distribution. They may even reflect the pattern of filaments and voids that are seen in deep space galactic surveys (Waxman et al. 1996). However, if the origin of the highest energy cosmic rays is due to decay of topological defects (Bhattacharjee 1992, Bhattacharjee 1995), then the anisotropy may have no relation to the distribution of visible matter in the universe.

## 2. The Fly’s Eye Experiment

The Fly’s eye experiment consisted of two detectors ( F.E. I and F.E. II ) located at Dugway Proving Ground (40° North) in Utah. The two detectors were spaced 3.4 km apart. Details of the experimental technique can be found in (Baltrusaitis et al. 1985, Cassiday 1985, Huang 1996). Briefly, UHE cosmic rays entering the atmosphere form an extensive air shower (EAS). The ionizing particles in this shower excite Nitrogen fluorescence in the atmosphere. Isotropically emitted light from this fluorescence is collected by spherical mirrors and detected by photomultipliers located at the two detector sites. The photomultiplier tube signals can be used to determine the geometry of the EAS ( i.e. its distance from the detector and arrival direction) and the energy of the primary particle. F.E. I had a larger aperture than F.E. II and events seen by it fall into the monocular data set. Events seen simultaneously by F.E.II ( which had a more limited aperture) were classified as stereo events. About 1/3 of the monocular data set was also seen in stereo. Because events seen in stereo have redundant measurements, the typical stereo geometrical and energy resolution is significantly better than that which is purely monocular. In order to have acceptable resolution, monocular data must be subjected to a number of cuts. The present data sample is large enough so that there is still statistical power even after the relatively stringent cuts required.

## 3. Data selection and angular resolution

All the Fly’s Eye data used in this analysis must pass a minimum standard cut which cuts out events with variables outside their natural range, or that have error greater than one half of their range or have relative error greater than 10.0 (Huang 1996).

In this study, we try to minimize the angular resolution while keeping the number of events as large as possible. We are guided by a Monte-Carlo simulation using a two source model of proton showers and iron showers. This model gives results consistent with the Fly’s Eye spectrum and composition results previously reported (Bird et al. 1994, Bird et al. 1993b, Bird et al., 1993d). These simulated events then pass the same event reconstruction programs as the real data. The reconstructed value and the input value for different variables are then compared. The angular error is defined as the space angle between the input shower direction and the reconstructed one. The tighter the data cut used, the fewer events remain. The optimization is to maximize the ratio of the relative decrease of angular error and the relative decrease of the number of events.

The most important factor controlling the angular error of monocular events is the shower track length. An event with longer track length has more degrees of freedom to determine arrival direction and, therefore, it has less angular error. We find the optimal track length is  $\geq 50^\circ$ .

The data are separated into six energy intervals E1 :  $0.2 - 0.4 EeV$ , E2:  $0.4 - 1.0 EeV$ , E3 :  $1.0 - 3.2 EeV$ , E4 :  $3.2 - 10.0 EeV$ , E5 :  $> 10.0 EeV$ , and E6 :  $> 32 EeV$ . According to the two source model, E1 should correspond to an almost pure iron composition while E5 and E6 consist of almost pure protons. The width of each energy interval is about half a decade, so we choose the relative energy error  $\leq 3.0$ .

A bracket of depth at shower maximum,  $X_{max}$ , is also applied

$$300 + 80. \times \log_{10}(E) < X_{max} < 1100 + 80. \times \log_{10}(E)$$

where  $E$  is the energy in  $EeV$ . Events outside this bracket have poorly reconstructed shower profile and large angular errors. The relative error of  $X_{max}$  is set at 1.0. We also apply a zenith angle cut at  $\leq 80^\circ$ .

The Fly’s Eye detectors operate on moonless nights. A weather code (Huang 1996) was recorded for every hour of observation. We required data to have been taken when less than 1/4 of the sky is cloudy.

Since we don’t know the actual arrival direction of real events, we cannot define the angular error as in Monte-Carlo simulated data. We use the uncertainty of the reconstructed value, i.e. the uncertainty in zenith angle  $d\theta$  and error in azimuth angle  $d\phi$ . An overall angular uncertainty is defined as

$$\delta = \sqrt{d\theta^2 + (\sin \theta \times d\phi)^2}$$

This value also shows a strong dependence on track length. Statistically, the mean angular uncertainty is related to the angular error (Huang 1996). But it is impossible to predict

angular error from angular uncertainty on an event by event basis. A cut at  $15^\circ$  on angular uncertainty is applied to the data.

The tight cuts we used in this study are listed in table 1. The resulting number of events of mono and stereo data are listed in table 2. Because the stereo data have only two events at energy  $> 32EeV$ , this analysis does not apply to this energy bin.

From Monte-Carlo studies, the angular resolution is  $3.2^\circ$  for monocular data and is  $1.1^\circ$  for stereo data at the 50% confidence level. At the 90% confidence level, the angular resolution is  $9.6^\circ$  for monocular data and is  $3.2^\circ$  for stereo data.

For the stereo subsample, we can compare the same event reconstructed by monocular and stereo methods. The space angle between these two direction is also a measure of the possible angular resolution of this subset of data. Figure 1 shows the resulting Poisson like distribution of angular resolution. At 50% confidence level, the angular resolution is approximately  $5.^\circ$ . In the large scale anisotropy analysis, in order to have enough statistics in each bin, we choose a bin width of 10 degrees for both monocular and stereo data.

#### 4. Isotropic background prediction

The background expected from an isotropic intensity can, in principle, be calculated by

$$B(l, b, E) = \sum_{\text{operation nights}} \int_{T_{\text{on}}}^{T_{\text{off}}} R(T) \times A(\theta, \phi, E) dT$$

where  $B(l, b, E)$  is the predicted isotropic background at longitude  $l$  and latitude  $b$  at energy  $E$  and  $R(T)$  is the event rate at time  $T$ . Note that  $\theta$  and  $\phi$  are here regarded as functions of  $l, b$  and  $T$ .  $A(\theta, \phi, E)$  is the acceptance of the detector, the geometric efficiency which is the relative ability to detect events of energy  $E$  from a certain zenith angle  $\theta$  and azimuth angle  $\phi$ .

Although the Fly’s Eye PMT singles rate is kept constant, the real event rate fluctuates due to variations in night sky noise and weather condition. Instead of using this integration, we use a scrambled event method to determine the isotropic background with better accuracy.

From the real data, we select the events that pass the weather code cut and store their trigger time in a time data bank. For those events that pass the tight cuts, we store their arrival direction  $(\theta, \phi)$  in a direction data bank. The time data bank contains information on the system on/off time and trigger rate  $R(T)$ . The direction data bank contains the

acceptance information. Then a simulated event is generated by randomly sampling a set of  $(\theta, \phi)$  from direction data bank and an event trigger time from time data bank. This randomization destroys the correlation from any source. The simulated events thus represent an expected data set if cosmic rays are isotropic.

Because of changes to the Fly’s Eye hardware, the acceptance may be different for different operation epochs. The background is calculated using the time and direction data from the same epoch. However, at energy  $> 3.2EeV$ , the number of events is so small that the acceptance becomes indistinguishable between epochs. In order to have proper statistics, we have to combine all epochs to form a direction data bank for this energy range.

In this study, we simulate 5,000 sets of data each having the same number of events as real data. The mean value of those 5,000 sets is used as the expected detector exposure. The fluctuation of those 5,000 sets represents the uncertainty in the exposure.

## 5. Broad scale anisotropy analysis

We compare the arrival direction distributions for two zones of the sky. The first zone is the whole sky while the second zone is the half of the sky ( $30^\circ < l < 210^\circ$ ) where the Fly’s Eye acceptance covers most of the galactic latitude. We also compare the distribution in supergalactic coordinates.

The null hypothesis of this study is that cosmic rays are isotropically distributed. Based on this hypothesis, we simulate the expected sky distribution and then compare it with the real data distribution. The data and background are binned in  $10^\circ$  latitude bins and the  $\chi^2$  of data vs background are calculated. We define

$$\begin{aligned} \chi^2 &= \sum_{i=1,\mu} (D_i - B_i)^2 / S_i^2 \\ D_i &= \text{number of events in energy } E \text{ and latitude bin } i \\ B_i &= \text{number of events of isotropic background} \\ S_i &= \text{standard deviation of } B_i \\ \mu &= \text{degrees of freedom} \end{aligned}$$

The probability of having a greater or equal  $\chi^2$  due to fluctuation in an isotropic distribution is also computed. A large probability shows that two distributions are similar to each other and therefore consistent with the null hypothesis. Conversely, a small probability shows that two distributions are incompatible. Table 3 lists the  $\chi^2$  and probability  $P(> \chi^2, \mu)$ .

The probability  $P(> \chi^2)$  indicates that some energy intervals may be inconsistent with

the isotropic expectation. To find a functional form of this anisotropy, we fit the data to two assumptions. First we look for a North-South anisotropy in the latitude  $b_i$  (GRAD fit)

$$R(b_i) = 1 + f \times b_i$$

Second we look for an excess from the galactic plane using a plane enhancement factor (WWFE fit)

$$R(b_i) = 1 - f + f \times c \times e^{-b_i^2}$$

where  $c$  is a normalization constant. Wolfendale and Chi (Chi et al. 1993) claim that  $c$  is 1.402, however, according to our calculation,  $c$  should be 1.437 (Huang 1996). Here we use  $c = 1.437$ .

The fitting is by minimizing  $\chi^2$  defined by

$$\chi^2 = \sum_{i=1,N} \frac{(D_i - A_i)^2}{E_i^2}$$

where

$$\begin{aligned} N &= \text{number of available bins (bins that have } B_i \neq 0), \\ A_i &= \text{number of expected events in latitude bin } i, A_i = B_i \times R(b_i) \\ E_i &= \text{error of } A_i \end{aligned}$$

The fluctuation of the expected number of events,  $S_i$ , based on the scrambled event method, does not follow a Poisson distribution exactly. We find that  $S_i$  is approximately 93% - 95% of  $\sqrt{B_i}$  the expected Poisson error. The two can be related by a quadratic form

$$k \times S_i^2 + S_i - \sqrt{B_i} = 0$$

where  $k$  depends on whether we use monocular or stereo data and the sky zones. When  $B_i$  is small,  $S_i$  approaches  $\sqrt{B_i}$ .  $E_i$  can be calculated by solving

$$\begin{aligned} k \times E_i^2 + E_i - \sqrt{A_i} &= 0 \\ E_i &= \frac{-1 + \sqrt{1 + 4k\sqrt{A_i}}}{2k} \end{aligned}$$

Figure 2 shows the difference  $S_i - \sqrt{B_i}$ . We also show the best fit to the above quadratic form. We use this relation to find the error  $E_i$  for any given  $A_i$ .

To determine if the data requires a particular functional form (GRAD or WWFE), we perform an F-test on the difference of  $\chi^2$ .

$$F = \frac{\chi_0^2 - \chi_{min}^2}{\chi_{min}^2 / dof}$$

where

$$\begin{aligned}
 \chi_0^2 &= \text{original } \chi^2 \text{ without functional form } (R(b) = 1) \\
 \chi_{min}^2 &= \chi^2 \text{ of best fit} \\
 \text{dof} &= \text{degrees of freedom}
 \end{aligned}$$

The number of degrees of freedom equals N-1 for the full sky zone and the supergalactic zone. For the half sky zone, we need to take out one more degree of freedom to normalize the total number of events. The probability of the F-test  $Prob(F; 1; dof)$  is then calculated. A small probability suggests the functional form is necessary.

The error of the fit parameter  $f$  is calculated by a similar process. The upper and lower bounds on  $f$  are the values of  $f$  at  $\chi_{min}^2 + 1$ . The error  $df$  is then calculated as one half of the difference of the upper and lower bound.

The same procedures are applied to the 5,000 simulated data sets. The result of these fits provides a check on the systematic error of the fit procedure. The significance of the fit to the data ( $f_{data}$ ) should be compared to the mean fitted value ( $f_{mean}$ ) and standard deviation ( $f_{sd}$ ) of fitted value of all simulated data sets. Then  $\sigma$  is defined as

$$\sigma = \frac{f_{data} - f_{mean}}{f_{sd}}$$

A single side Gaussian probability of this  $\sigma$  is also calculated

$$P_{gauss} = \frac{1}{\sqrt{2\pi}} \int_{\sigma}^{\infty} e^{-\frac{z^2}{2}} dz$$

To compare the data with the simulated data sets, a probability of having a greater fitted value is calculated by

$$P_{sim}(> f_{data}) = \frac{\# \text{ of data sets that generate } f > f_{data}}{\text{total } \# \text{ of data sets}}$$

The total number of simulated data sets is 5,000. Figure 3 shows the histogram of the WWFE fit parameter  $f_E$  for the simulated isotropic data sets. The distribution of fit parameters can be fitted to a Gaussian form. This figure shows the statistical fluctuation of an isotropic background. The fit parameter for the real data,  $f_{data}$ , is shown by the solid arrow.

A small value of probability ( $P < 0.05$ ) suggests the fit parameter is large compared to the fluctuation of isotropic background. A large value ( $P > 0.95$ ) suggests that the fit parameter is small.

Tables 4 thru 7 list the fit results in galactic coordinates. Tables 8 and 9 list the fit results in supergalactic coordinates. Figure 4 thru 9 show the fit results for various conditions.



## 6. Discussion

### 6.1. Systematic error:

Due to the limited coverage of galactic latitude, the isotropic background does not always produce a null plane enhancement factor or gradient. However, the systematic bias is negligible at energies  $< 3.2EeV$ . The systematic bias is higher at energy  $> 3.2EeV$  and the fit parameter may not be the true magnitude of the anisotropy. However, the significance and probability are not affected by this bias, because the data is compared with simulated data sets. The probabilities quoted in the latter part of this article all come from  $P_{sim}$ .

We also make a study of the systematic bias by reducing the number of events in each energy bin and redoing the fitting. Figure 10 shows the distribution of fit parameters and background as a function of total number of events. This study shows that the fit result does not depend strongly of event number. However when the number of event falls below 100, the isotropic background begins to give  $f_E$  significantly different from 0. This shows the systematic bias is an effect of low statistics. We suspect the large negative  $f_E$  reported in some studies (Chi et al. 1993) could also be affected by the large bias due to low statistics.

The other systematic effect is that the error is not Poisson distributed. If we use the square root of the expected number  $\sqrt{B_i}$  as the error, we will over-estimate the error in higher event count regions, galactic latitude  $-25^\circ$  to  $65^\circ$ . By using the fitted error, we improve both the  $\chi^2$  value and the accuracy of the fit.

### 6.2. Anisotropy in galactic coordinates:

To search for anisotropy, we first look at the  $\chi^2$  between data and isotropic background. The  $P(> \chi^2, \mu)$  in table 10 shows that E2 has  $P(> \chi^2, \mu)$  less than 0.20 for all data. This may indicate that the data distribution is inconsistent with an isotropic background. On the other hand, for E4, all the  $P(> \chi^2, \mu)$  are larger than 0.5, This might suggest the cosmic ray distribution at E4 is consistent with an isotropic background.

The most significant result is the WWFE fit for E2 ( $0.4 - 1.0EeV$ ). The significance varies from 0.031 to 0.002. Both mono and stereo data give the fit plane enhancement factor  $f_E$  at about 0.10. The F-test probabilities, 0.012 for mono and 0.108 for stereo, also show that such a WWFE fit indeed reduces the  $\chi^2$ . A non-zero  $f_E$  is needed to fit the data. Finally, the isotropic background has a chance probability  $P_{sim} = 0.002$  for mono data and 0.016 for stereo data to produced  $f_E$  larger than the  $f_E$  of the data. The gradient fit

produces  $P_{sim} = 0.731$  to  $0.952$  or  $\sim 2\sigma$ , which is not sufficiently significant. The data thus supports a small anisotropy in E2 ( $0.4 - 1.0 EeV$ ). Figure 11 shows the number of events, event rate, and significance in the E2 bin.

Table 10 lists the probability values of all the fits. The table shows that most of the fits have similar probability for full sky and half sky zones except the WWFE fit to stereo data at E3. Similar result can be found for mono and stereo data except for the E1 gradient fit and the E4 WWFE fit.

Based on previous FE results on spectrum and composition, we expect that the anisotropy in the energy range below  $3.0 EeV$  may be different from that of the higher energy flux. The lower energy data appears to be of a heavier composition and is likely to be of a galactic origin. We can separate data into two groups: group 1, E1-E3 Energy  $< 3.2 EeV$  and group 2, E4-E6 energy  $> 3.2 EeV$ . We use compound probability (Fisher 1958, Eadie et al. 1971) to combine probabilities in table 10. The results are listed in table 11.

$$\begin{aligned} p' &= P(E1) \times P(E2) \times P(E3) \\ CP &= p' \times (1. - \log(p') + \frac{1}{2}(\log p')^2) \end{aligned} \tag{1}$$

Table 11 show that group 1 supports a positive  $f_E$  at approximately  $3.2 - 3.3\sigma$  for monocular data and  $1.4 - 1.9\sigma$  for stereo data. This result suggests that cosmic rays with energy  $< 3.2 EeV$  may have a small anisotropy related to the galactic plane. The stereo data has a less significant anisotropy because of a very small  $f_E$  and large probability at E1 ( $0.2 - 0.4 EeV$ ). Detailed comparison between mono data and stereo data shows that there is in fact an excess of events near the galactic center in the mono data. However, the stereo data acceptance is small in this region due to smaller zenith angle coverage. For the galactic latitude gradient, the compound probabilities are in disagreement between monocular data and stereo data.

For group 2, both mono and stereo data have no signs of galactic plane enhancements. The gradient fit shows nothing significant again. Cosmic rays with energy  $> 3.2 EeV$  are consistent with an isotropic background. Due to the low statistics and large background bias for energy  $> 10 EeV$ , we can not prove any anisotropy in this energy region.

### 6.3. Anisotropy in supergalactic coordinates:

Table 12 lists the probability  $P_{sim}$  of mono and stereo data in supergalactic coordinates. Although the E2  $f_E$  fit has a  $P_{sim} = 0.9924$ , (approximately  $-2\sigma$ ), the event distribution

shows that the excess of events comes from supergalactic latitude  $> +70^\circ$  or  $< -70^\circ$ , i.e. regions where an excess from the galactic plane could be having a strong effect. This supergalactic polar excess is not significant either in individual bin (E2 mono data  $2.38\sigma$ ) or over three energy bins (E1-E3). Contrary to the Stanev et al. (Stanev et al., 1995) result, we do not see evidence of anisotropy coming from the supergalactic plane for energies  $> 10EeV$ . However, this result is consistent with Kewley et al. (Kewley 1996). They did not find excess of supergalactic plane in the southern sky either.

#### 6.4. Comparison with other results

Most ground array experiment use harmonic analysis to look for anisotropy. However, the Fly’s Eye does not have uniform coverage in Right Ascension and this makes harmonic analysis difficult to interpret.

There had been several reports on the anisotropy toward the galactic plane. Gillerman & Watson (Gillerman & Watson 1993) combined several groups data on  $f_E$  and calculate the  $\chi^2$  for a null fit ( $f_E = 0$ ). They report a  $\chi_\mu^2 = 2.2$  or a probability of 0.9% that  $f_E$  is consistent with zero. There may be problems with possible different energy scales between these groups of data. In this study, we use the same data set, therefore there is no problem with energy cross-calibration. The overall result still supports an enhancement from the galactic plane.

Recently, the AGASA group reported a significant first harmonic at energy  $10^{17.9} - 10^{18.3}eV$ , with a chance probability of 0.005% (Hayashida et al. 1998). Considering the possible energy scale difference between the Fly’s Eye and the AGASA, this range may well overlap with our range  $10^{17.6} - 10^{18}eV$ . A detailed comparison of the two groups results is currently under study.

### 7. Summary

1. We reexamine both the monocular and stereo Fly’s Eye data and look for anisotropy related to galactic or supergalactic latitude. Two functional forms are studied. The first is the latitude gradient

$$I(b) = I_0(1 + f \times b)$$

the second is plane enhancement factor

$$I(b) = I_0(1 - f + 1.437 \times f \times e^{-b^2}).$$

2. The isotropic background is calculated by scrambling the event arrival direction and trigger time. There are 5,000 simulated data sets, each having the same number of events as the real data. The mean value of these 5,000 sets are used to represent the distribution expected from isotropy. The standard deviation of these 5,000 sets is used as the uncertainty in that distribution.
3. We find that the galactic plane enhancement factor  $f_E$  is non-zero at the  $3.2\sigma$  level for energies  $< 3.2EeV$ . The chance probability of such an anisotropy existing in these 3 energy bins is less than 0.06%. For energy  $> 3.2EeV$ , although a negative plane enhancement factor could be possible, the significance is less than  $2\sigma$ . The galactic latitude gradient is only significant in the energy range  $0.4 - 1EeV$  where the galactic plane enhancement is strongest too. Overall, the galactic latitude gradient is not as significant as the galactic plane enhancement factor. One should bear in mind that the actual form of the anisotropy may be different from either the WWFE or GRAD functions.
4. No significant supergalactic latitude gradient or supergalactic plane enhancement factor is found.
5. This analysis supports the the view that the arrival directions of cosmic rays at energies  $< 3.2EeV$  are weakly correlated with the galactic plane. For energy  $> 3.2EeV$ , no significant anisotropy is found.

We acknowledge the Department of the Army and the staff of Dugway Proving Ground for their cooperation and assistance. This work has been supported in part by the National Science Foundation (at Utah) and the U.S. Department of Energy (at Illinois).

Table 1. Tight cuts used in this study.

Parameter	Requirement
track length	$\geq 50^\circ$
zenith angle	$\leq 80^\circ$
angular uncertainty $\delta^a$	$\leq 15^\circ$
relative error in energy	$\leq 3.0$
relative error in $X_{max}$	$\leq 1.0$
$X_{max}$	$300 + 80 \times \log(Energy) \leq X_{max} \leq 1100 + 80 \times \log(energy)$
weather	No frost, moderate or no scattering, $< 1/4$ sky cloudy

<sup>a</sup>angular uncertainty  $\delta = \sqrt{d\theta^2 + (\sin \theta \times d\phi)^2}$

Table 2. Number of events and mean energy of events that pass the tight cuts

	Energy ( $EeV$ )	Stereo		Mono	
		Num	$\langle E \rangle$	Num	$\langle E \rangle$
E1	0.2 – 0.4	2709	0.289	5183	0.287
E2	0.4 – 1.0	2402	0.619	4815	0.621
E3	1.0 – 3.2	1141	1.613	2465	1.658
E4	3.2 – 10.0	191	5.912	597	5.357
E5	> 10.0	33	16.366	169	22.806
E6	> 32.0	2	41.786	17	78.282
Total		6476		13229	

Table 3. The  $\chi^2$  for data  $D_i$  and isotropic background  $B_i$ .

Zone	Energy	Num. of events	$\mu$	$\chi_\mu^2$	Mono $P(> \chi^2, \mu)$	Num. of events	$\mu$	$\chi_\mu^2$	Mono $P(> \chi^2, \mu)$
Galactic latitude:									
Full sky	E1	5183	17	1.105	0.341	2709	17	0.715	0.790
	E2	4815	17	1.355	0.148	2402	17	1.673	0.040
	E3	2465	17	1.290	0.187	1141	17	0.830	0.659
	E4	597	17	0.631	0.870	191	17	0.910	0.561
	E5	169	17	0.988	0.468	33	16	0.714	0.791
	E6	17	16	0.923	0.545				
Half sky	E1	4553	16	1.312	0.179	2289	16	0.738	0.757
	E2	4092	16	1.430	0.117	2031	16	1.279	0.200
	E3	2040	16	1.071	0.377	972	16	0.655	0.840
	E4	470	16	0.761	0.731	152	16	0.820	0.664
	E5	130	16	0.928	0.535	24	15	0.631	0.862
	E6	14	15	1.000	0.453				
Supergalactic latitude:									
	E1	5183	17	0.919	0.551	2709	17	1.780	0.025
	E2	4815	17	1.567	0.064	2402	17	0.601	0.894
	E3	2465	17	1.313	0.173	1141	17	0.620	0.879
	E4	597	17	1.090	0.356	191	17	0.757	0.745
	E5	169	17	1.278	0.195	33	17	0.915	0.556
	E6	17	17	0.727	0.778				

Table 4. Results for WWFE fitting using the full sky data. P(F) is the F-test probability  $Prob(F; 1; dof)$ .

E	Data	$f$	$df$	$\chi^2_{min}$	F	P(F)	$f_{mean}$	$f_{SD}$	$P_{gauss}$	$P_{sim}$
E1	mono	0.067	0.035	0.943	3.922	0.065	-0.003	0.037	0.030	0.029
	stereo	0.016	0.047	0.753	0.151	0.702	-0.003	0.050	0.352	0.354
E2	mono	0.104	0.036	0.955	8.120	0.012	-0.002	0.038	0.003	0.002
	stereo	0.109	0.052	1.505	2.896	0.108	-0.004	0.054	0.018	0.016
E3	mono	0.063	0.052	1.279	1.145	0.300	-0.004	0.056	0.116	0.116
	stereo	0.079	0.080	0.823	1.152	0.299	-0.008	0.077	0.128	0.132
E4	mono	-0.072	0.113	0.645	0.635	0.437	-0.016	0.111	0.694	0.705
	stereo	-0.049	0.183	0.963	0.075	0.787	-0.044	0.195	0.511	0.514
E5	mono	-0.264	0.218	0.954	1.616	0.222	-0.061	0.225	0.817	0.818
E5	ste	-0.576	0.402	0.631	3.235	0.091	-0.232	0.454	0.776	0.774
E6	mono	-1.263	0.447	0.618	9.379	0.007	-0.243	0.580	0.961	0.959



Table 5. Results for WWFE fitting using the half sky data.

E	Data	$f$	$df$	$\chi_{min}^2$	F	P(F)	$f_{mean}$	$f_{SD}$	$P_{gauss}$	$P_{sim}$
E1	mono	0.096	0.040	1.016	5.659	0.031	-0.003	0.042	0.009	0.008
	stereo	0.045	0.056	0.745	0.864	0.367	-0.006	0.058	0.194	0.196
E2	mono	0.126	0.043	0.972	8.539	0.011	-0.003	0.045	0.002	0.002
	stereo	0.113	0.061	1.144	2.879	0.110	-0.006	0.063	0.029	0.031
E3	mono	0.024	0.060	1.132	0.137	0.716	-0.007	0.064	0.318	0.317
	stereo	-0.039	0.093	0.687	0.252	0.623	-0.014	0.091	0.608	0.615
E4	mono	-0.156	0.130	0.715	2.042	0.173	-0.026	0.131	0.839	0.844
	stereo	0.098	0.215	0.862	0.233	0.636	-0.073	0.228	0.227	0.226
E5	mono	-0.261	0.252	0.915	1.230	0.285	-0.094	0.261	0.739	0.737
	stereo	-0.486	0.454	0.596	1.941	0.184	-0.319	0.509	0.629	0.627
E6	mono	-1.448	0.428	0.608	11.313	0.004	-0.323	0.668	0.954	0.959

Table 6. Results for gradient fitting using the full sky data.

E	Data	$f$	$df$	$\chi_{min}^2$	F	P(F)	$f_{mean}$	$f_{SD}$	$P_{gauss}$	$P_{sim}$
E1	Mono	-0.050	0.021	0.832	6.569	0.021	-0.001	0.022	0.987	0.985
	stereo	0.040	0.029	0.638	3.077	0.099	-0.001	0.028	0.074	0.072
E2	Mono	-0.021	0.023	1.385	0.628	0.440	-0.001	0.023	0.811	0.803
	stereo	-0.053	0.030	1.582	1.975	0.179	-0.001	0.031	0.955	0.952
E3	Mono	-0.052	0.030	1.188	2.458	0.136	-0.001	0.031	0.947	0.947
	stereo	-0.098	0.043	0.576	8.507	0.010	-0.002	0.045	0.984	0.986
E4	Mono	0.072	0.064	0.589	2.229	0.155	-0.005	0.062	0.107	0.105
	stereo	0.066	0.105	0.943	0.417	0.528	-0.012	0.104	0.228	0.225
E5	Mono	-0.033	0.113	1.045	0.082	0.779	-0.016	0.125	0.555	0.547
	stereo	0.134	0.204	0.733	0.565	0.463	-0.021	0.245	0.263	0.257
E6	Mono	-0.114	0.191	0.961	0.341	0.567	-0.051	0.325	0.576	0.544

Table 7. Results for gradient fit using the half sky data.

E	Data	$f$	$df$	$\chi_{min}^2$	F	P(F)	$f_{mean}$	$f_{SD}$	$P_{gauss}$	$P_{sim}$
E1	Mono	-0.066	0.024	0.897	8.411	0.011	-0.001	0.024	0.997	0.997
	stereo	0.028	0.034	0.742	0.928	0.351	-0.001	0.033	0.193	0.191
E2	Mono	-0.017	0.026	1.497	0.286	0.600	-0.001	0.026	0.738	0.731
	stereo	-0.050	0.035	1.228	1.662	0.217	-0.001	0.035	0.919	0.920
E3	Mono	-0.026	0.034	1.106	0.491	0.494	-0.001	0.036	0.758	0.755
	stereo	-0.053	0.049	0.622	1.836	0.196	-0.001	0.052	0.841	0.843
E4	Mono	0.058	0.069	0.766	0.898	0.358	-0.003	0.072	0.198	0.197
	stereo	0.027	0.127	0.872	0.054	0.819	-0.002	0.120	0.403	0.398
E5	Mono	0.048	0.144	0.983	0.112	0.743	-0.011	0.143	0.339	0.339
	stereo	-0.058	0.267	0.670	0.071	0.793	0.017	0.281	0.606	0.597
E6	Mono	-0.133	0.215	1.042	0.352	0.562	-0.028	0.373	0.611	0.594

Table 8. Results for WWFE fitting using the supergalactic latitude.

E	Data	$f$	$df$	$\chi_{min}^2$	F	P(F)	$f_{mean}$	$f_{SD}$	$P_{gauss}$	$P_{sim}$
E1	mono	-0.004	0.038	0.975	0.013	0.910	-0.002	0.039	0.518	0.525
	stereo	-0.052	0.050	1.824	0.592	0.453	-0.004	0.052	0.824	0.827
E2	mono	-0.095	0.038	1.247	5.368	0.034	-0.002	0.038	0.992	0.991
	stereo	-0.051	0.052	0.580	1.634	0.219	-0.004	0.054	0.807	0.808
E3	mono	-0.019	0.052	1.387	0.094	0.763	-0.004	0.054	0.611	0.623
	stereo	-0.066	0.078	0.613	1.204	0.289	-0.008	0.077	0.775	0.770
E4	mono	-0.012	0.108	1.157	0.011	0.916	-0.015	0.108	0.488	0.487
	stereo	0.113	0.178	0.780	0.495	0.492	-0.039	0.185	0.206	0.204
E5	mono	0.075	0.203	1.350	0.101	0.755	-0.059	0.219	0.271	0.281
	stereo	-0.124	0.322	0.963	0.157	0.697	-0.206	0.430	0.425	0.439
E6	mono	-0.208	0.456	0.759	0.281	0.603	-0.239	0.569	0.478	0.475

Table 9. Results for gradient fit using the supergalactic latitude.

E	Data	$f$	$df$	$\chi_{min}^2$	F	P(F)	$f_{mean}$	$f_{SD}$	$P_{gauss}$	$P_{sim}$
E1	mono	0.001	0.021	0.976	0.003	0.954	-0.001	0.023	0.471	0.460
	stereo	-0.001	0.028	1.891	0.001	0.974	-0.001	0.030	0.500	0.489
E2	mono	0.005	0.021	1.661	0.033	0.858	-0.001	0.022	0.398	0.394
	stereo	0.017	0.030	0.617	0.557	0.466	-0.001	0.031	0.280	0.276
E3	mono	-0.047	0.029	1.235	2.071	0.169	-0.001	0.031	0.928	0.924
	stereo	0.000	0.043	0.659	0.000	1.000	-0.002	0.044	0.481	0.472
E4	mono	0.010	0.061	1.156	0.024	0.880	-0.004	0.061	0.408	0.400
	stereo	-0.065	0.103	0.780	0.493	0.493	-0.106	0.102	0.704	0.700
E5	mono	-0.273	0.119	1.048	4.736	0.045	-0.014	0.126	0.981	0.981
	stereo	0.168	0.265	0.945	0.454	0.510	-0.039	0.237	0.191	0.185
E6	mono	-0.178	0.250	0.742	0.662	0.428	-0.045	0.320	0.661	0.638

Table 10. The probability  $P_{sim>(> f_{data})}$  for all fits.

Energy	WWFE				GRAD			
	Mono		Stereo		Full	Half	Full	Half
	Full	Half	Full	Half				
E1	0.0292	0.0080	0.3544	0.1962	0.9852	0.9966	0.0722	0.1910
E2	0.0022	0.0022	0.0162	0.0312	0.8028	0.7308	0.9524	0.9196
E3	0.1162	0.3166	0.1316	0.6148	0.9472	0.7550	0.9860	0.8432
E4	0.7048	0.8438	0.5142	0.2258	0.1046	0.1968	0.2254	0.3976
E5	0.8178	0.7372	0.7744	0.6266	0.5474	0.3386	0.2574	0.5972
E6	0.9590	0.9590			0.5444	0.5942		

Table 11. The compound probability and sigma of all the fits.

	Mono				Stereo			
	Full CP	sig	Half CP	sig	Full CP	sig	Half CP	sig
	E1-E3				E1-E3			
WWFE CP	0.0006	3.2315	0.0005	3.3016	0.0257	1.9481	0.0834	1.3825
GRAD CP	0.9968	-2.7227	0.9771	-1.9968	0.4958	0.0106	0.7011	-0.5275
	E4-E6				E4-E5			
WWFE CP	0.9776	-2.0063	0.9843	-2.1525	0.7649	-0.7220	0.4182	0.2066
GRAD CP	0.3268	0.4489	0.3739	0.3216	0.2232	0.7615	0.5789	-0.1989

Table 12. The probability  $P_{sim}( > f_{data} )$  for all the fits in supergalactic latitude.

Fit Energy	WWFE		GRAD	
	Mono	Stereo	Mono	Stereo
E1	0.5246	0.8274	0.4602	0.4890
E2	0.9914	0.8076	0.3936	0.2762
E3	0.6234	0.7696	0.9240	0.4720
E4	0.4866	0.2040	0.4002	0.7000
E5	0.2806	0.4386	0.9810	0.1846
E6	0.4748		0.6382	
E1-E3 CP	0.8951	0.9700	0.7340	0.4808
Significance	$1.25\sigma$	$1.88\sigma$	$0.63\sigma$	$0.05\sigma$



## REFERENCES

- Baltrusaitis, R. M. et al., 1985, Nucl. Instr. Meth., A240, 410-428
- Bird, D. J. et al., 1993, proc. 23rd ICRC, Calgary, 2. 30
- Bird, D. J. et al., 1993, Proc. 23rd ICRC (Calgary), 2, 38
- Bird, D. J. et al., 1993, proc. 23rd ICRC, Calgary, 2. 55
- Bird, D. J. et al., 1993, Phys. Rev. Lett., 71, 3401,
- Bird, D. J. et al., 1994, Ap. J., 424, 491
- Bhattacharjee, P., Hill, C. T., & Schramm, D. N., 1992, Phys. Rev. Lett. 69, 567
- Bhattacharjee, P. & Sigl, G., 1995, Phys. Rev. D. 51, 4079
- Cassiday, G. L., 1985, Ann. Rev. Nucl. Part. Sci., 33, 321-349
- Chi, X. et al., 1993, J. Phys G, 19, 780
- Eadie, W. T., et al. 1971, Statistical Methods in Experimental Physics, North-Holland: Amsterdam, 283
- Fisher, R. A., 1958, Statistical Methods For Research Workers, 13th ed., Hafner: New York, 99
- Gillerman, M. S. & Watson, A. A., 1993, Proc. 23rd ICRC (Calgary), 2, 47
- Hayashida, N. et al., ICRR Preprint, 1998,
- Huang, M.A., 1996, Ph.D thesis, Univ. of Utah
- Kewley, L. J., Clay, R. W. & Dawson, B. R., 1996, Astropart. Phys. 5, 69
- Stanev, T. et al., 1995, Phys. Rev. Lett. 75, 3056
- Waxman, E., Fisher, K. B., & Piran, T., 1996, Astro. Astop. Apr
- Wdowczyk, J., & Wolfendale, A. W., 1984, J. Phys. G, 10, 1453
- Kronberg, P. P., 1994, Rep. Prog. Phys., 57, 325.

Fig. 1.— Angular resolution of common events in both mono and stereo data. The  $\Delta\Omega$  is the space angle between arrival directions reconstructed by monocular and stereo methods.

Fig. 2.— The X axis is  $\sqrt{B_i}$  the expected error from Poisson distribution. The Y axis is the difference between the observed scrambled event method standard deviation and the expected Poisson error  $S_i - \sqrt{B_i}$ , shown as crosses, and the fitted error difference  $E_i - \sqrt{B_i}$ , shown as circles.

Fig. 3.— Histogram of the WWFE fit parameter for monocular data using the full sky at energy of 0.4-1.0EeV. The probability  $P_{sim}$  is the histogram area from the fit parameter for the data ( $f_{data}$  solid arrow) to the right end of axis. Similarly, the  $P_{gauss}$  is the area of the fitted Gaussian form from the fit to the right end of the axis.

Fig. 4.— The WWFE fit using the full sky data.

Fig. 5.— The WWFE fit using the half sky data.

Fig. 6.— The gradient fit using the full sky data.

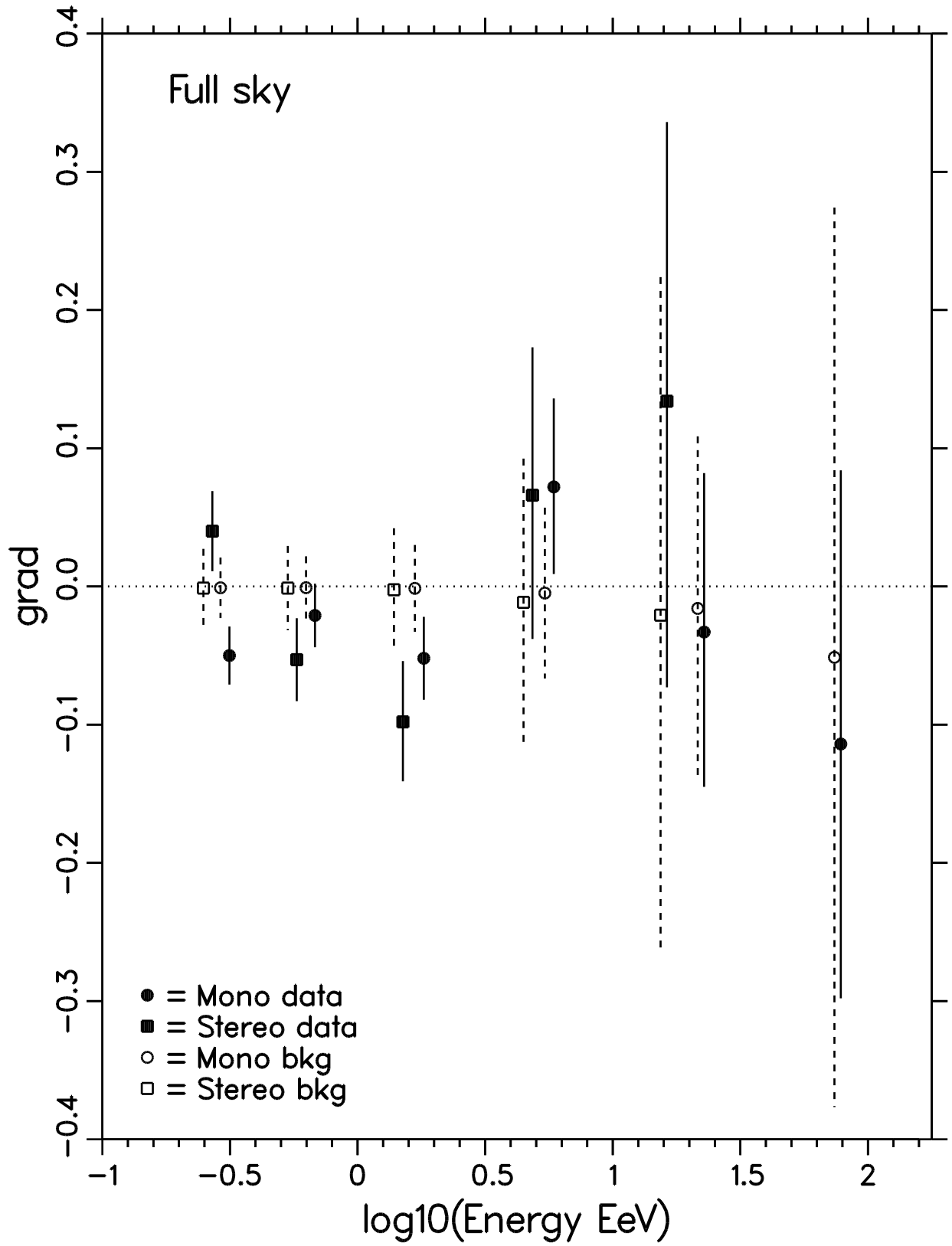
Fig. 7.— The gradient fit using the half sky data.

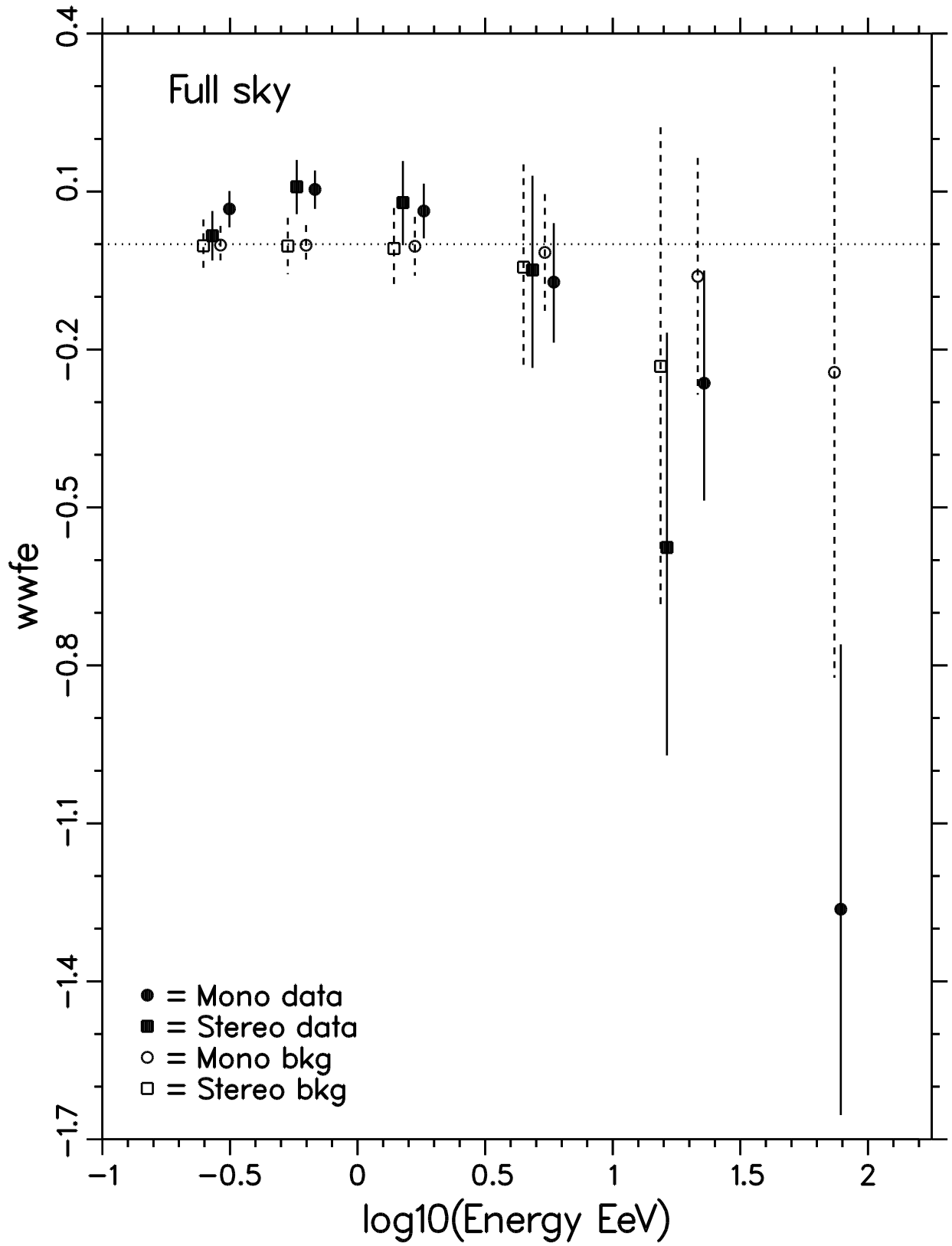
Fig. 8.— The WWFE fit using the supergalactic latitude.

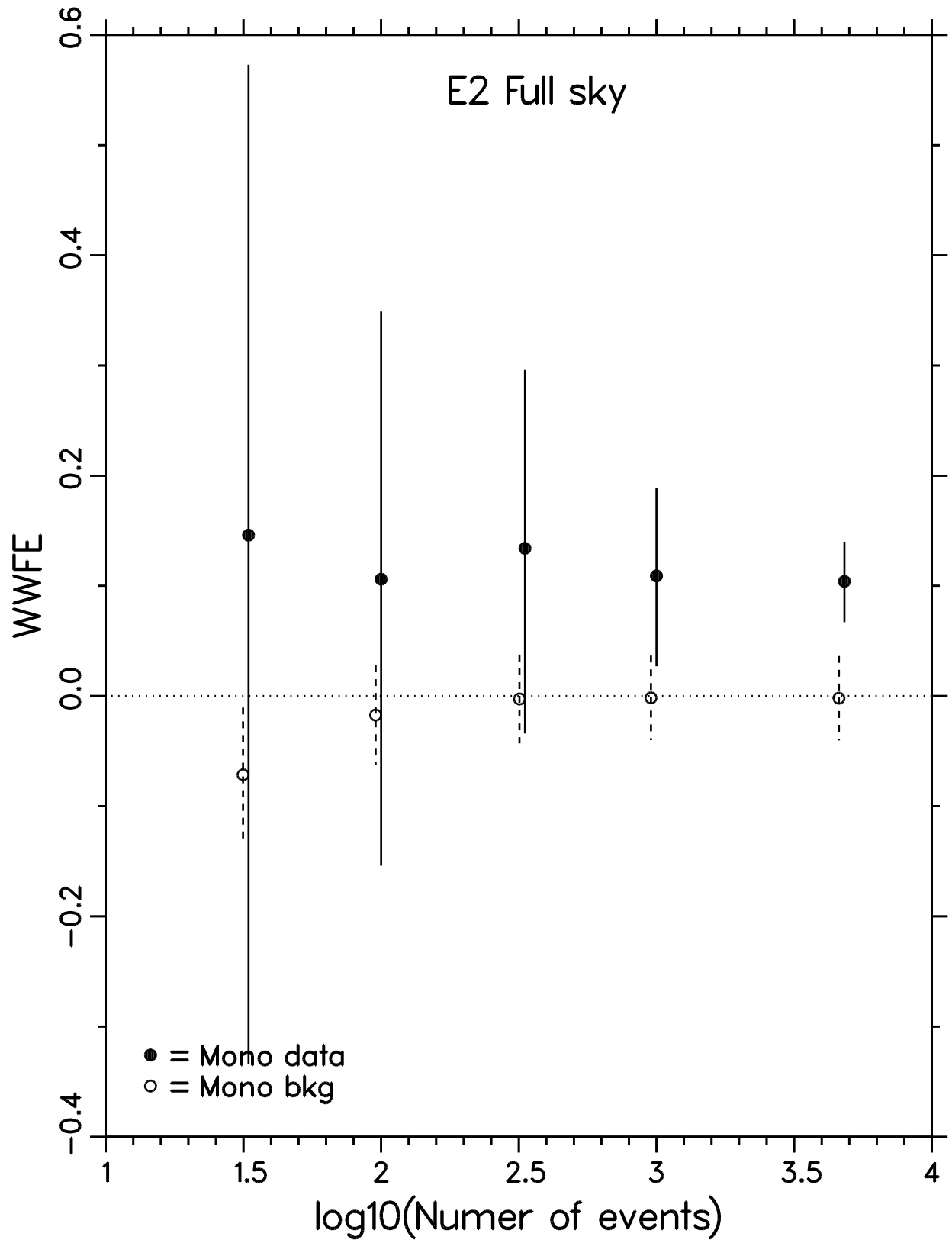
Fig. 9.— The gradient fit using the supergalactic latitude.

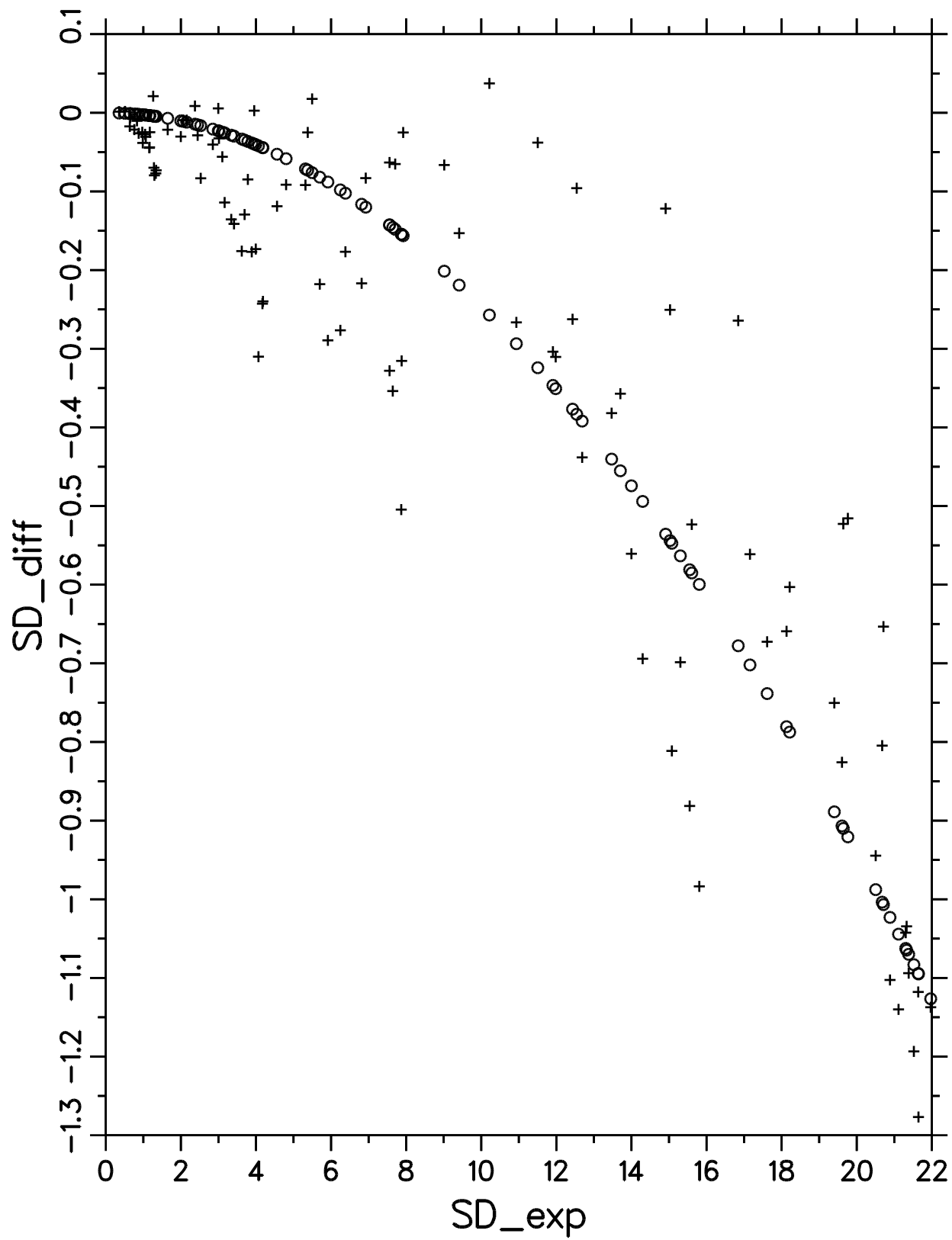
Fig. 10.— The WWFE fit of E2 monocular data. The total number of events are reduced from 4815 to 1000, 333, 100, and 33. The solid dots represent the data and mean value of the simulated background are given by circles.

Fig. 11.— Monocular data and isotropic background distribution of the all sky zone for 0.4-1.0EeV. The bottom figure shows the histogram of the number of events as function of galactic latitude. The data ( $D_i$ ) are represented by the histogram steps while the isotropic background ( $B_i$ ) is the dotted line. The middle figure show the event rate which is the ratio of number of events to background,  $D_i/B_i$ . The WWFE fit is shown by the dashed line and the gradient fit is shown by the dot-dashed line. The top figure show the significance  $(D_i - B_i)/S_i$ .

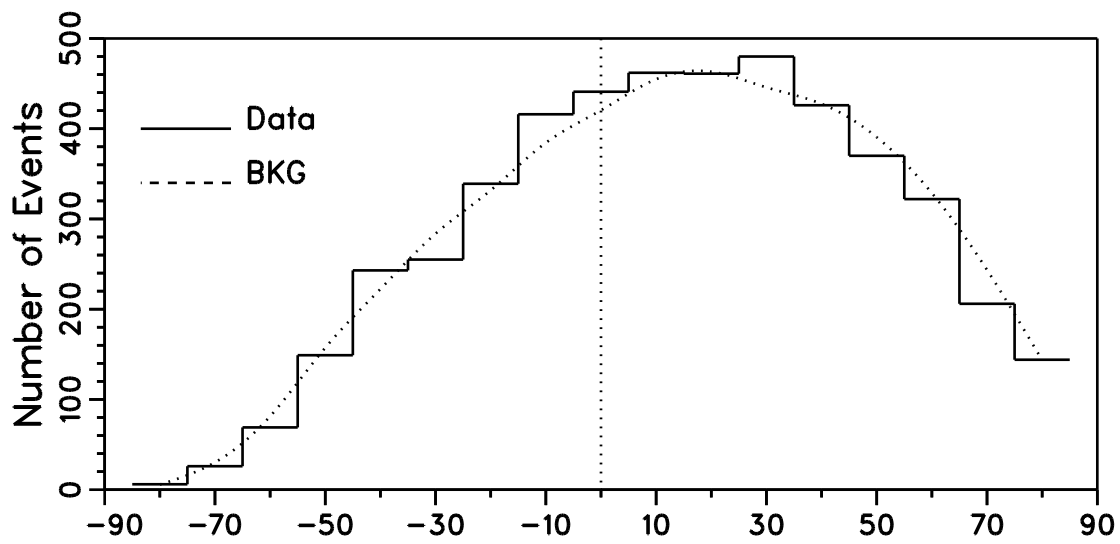
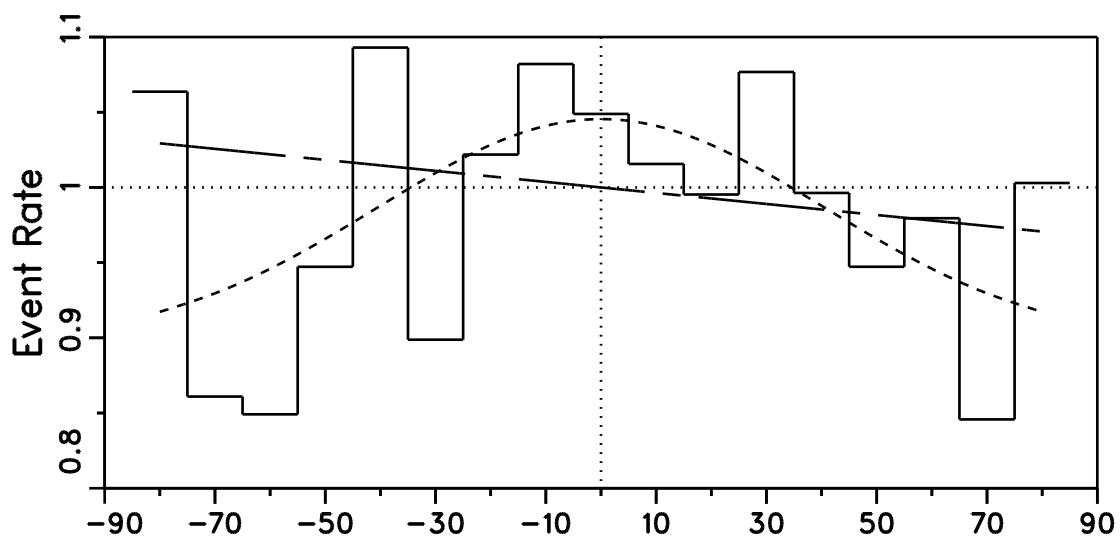
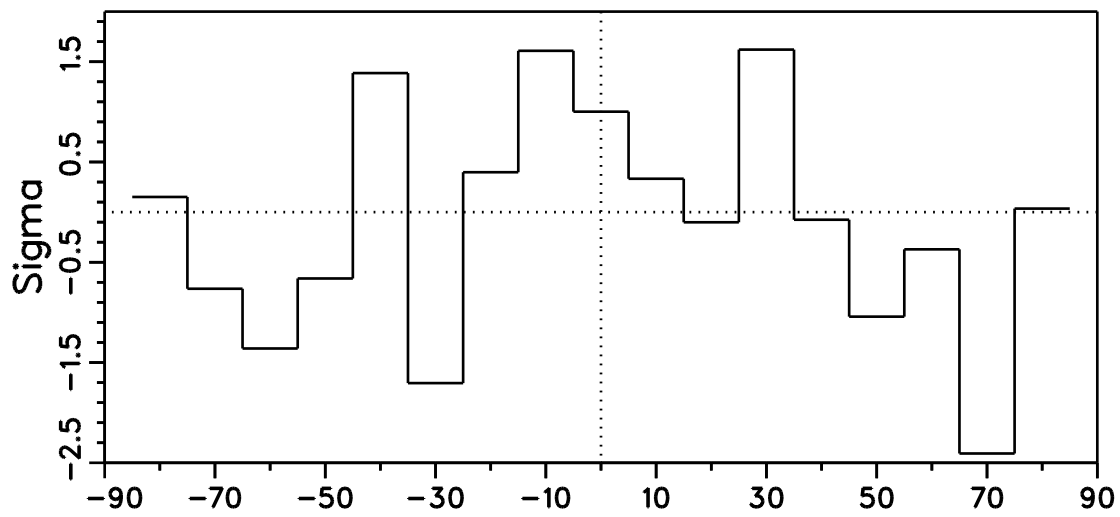






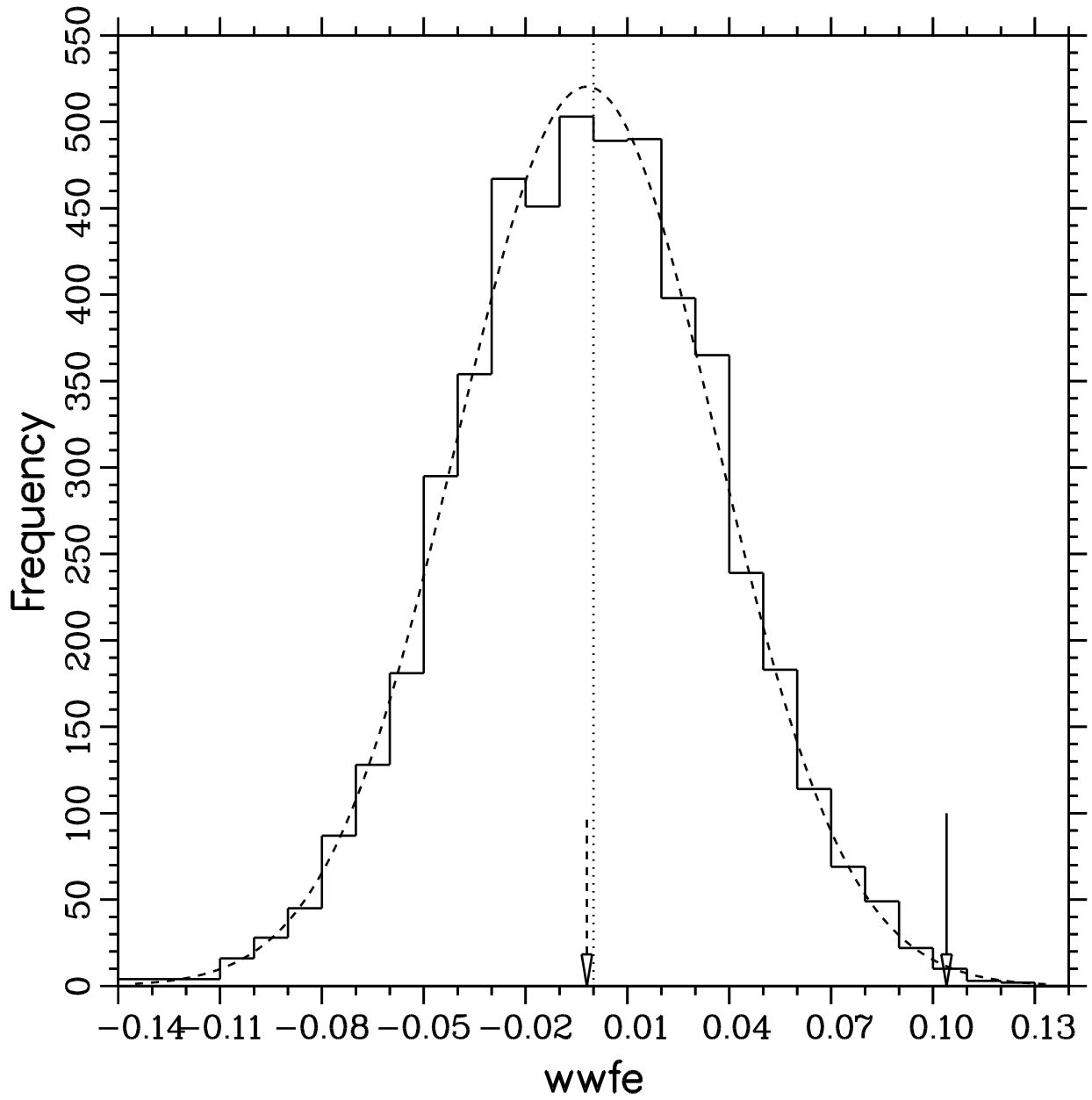


All sky



Galactic latitude (deg)

E2	N4815	DOF 17	Chi-sq 1.355	Prob 0.148
-----	WWFE=	0.104 +/-	0.036	Prob 0.002
-----	GRAD=	-0.021 +/-	0.023	Prob 0.803



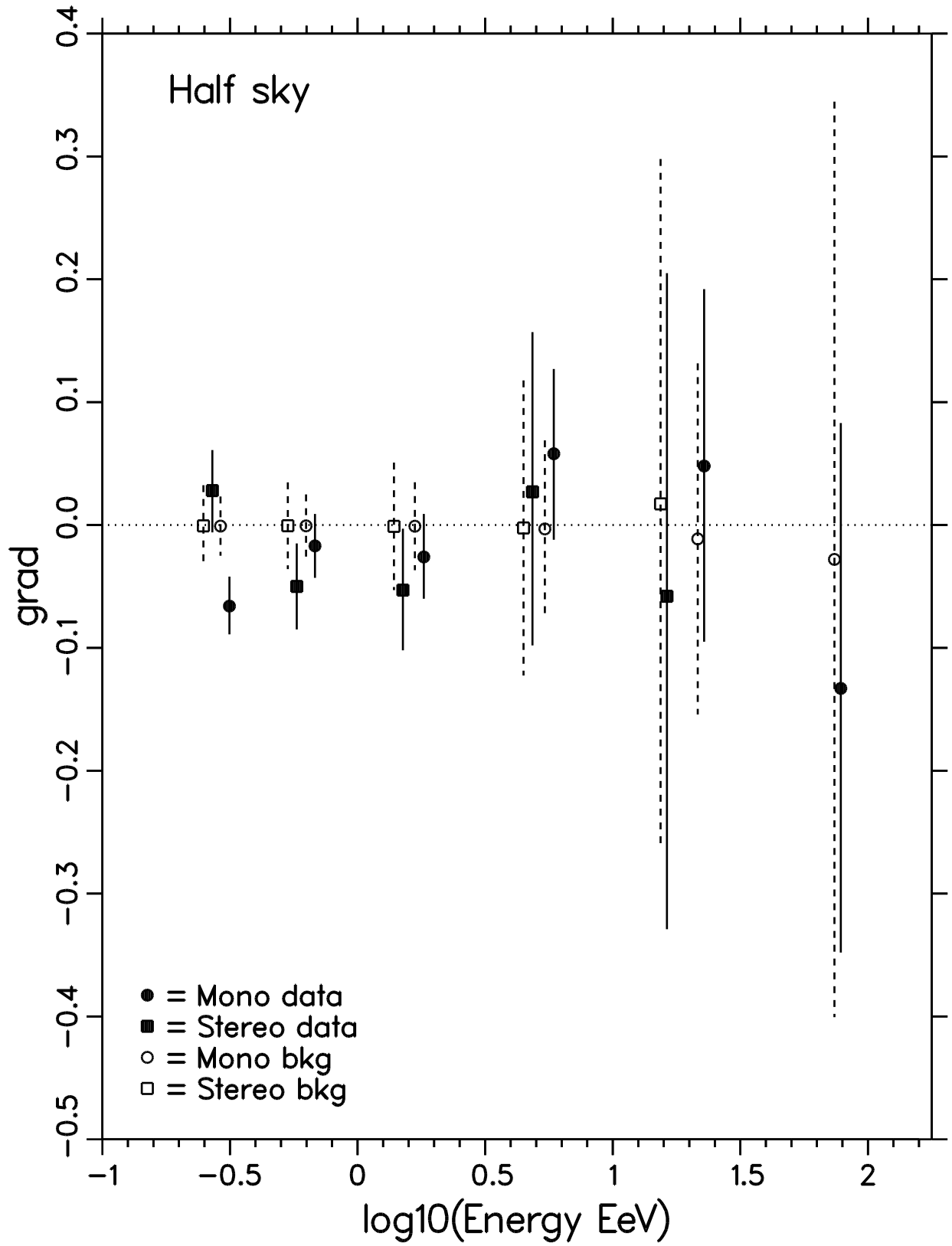
MEAN = -0.0020

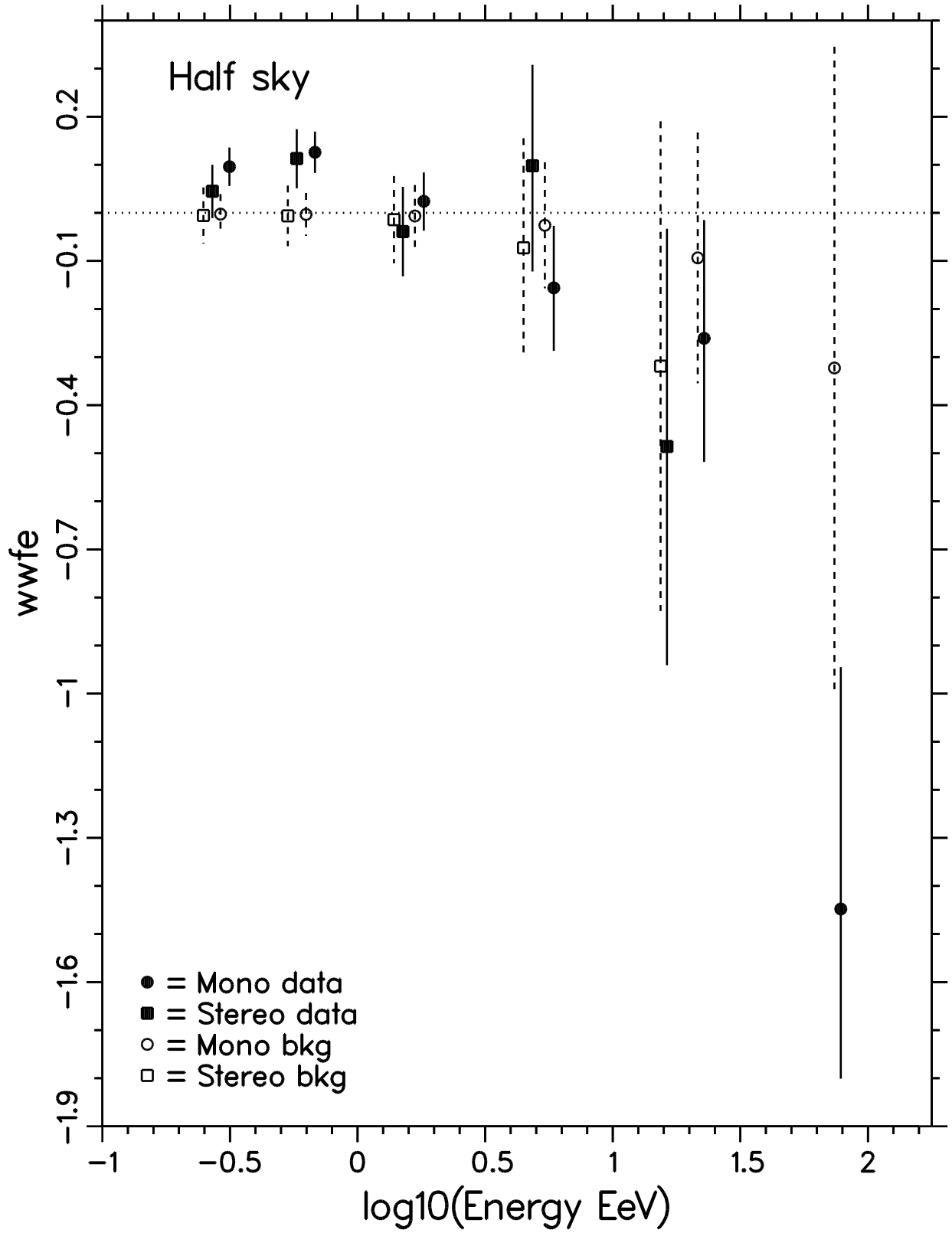
S.D. = 0.0383

wwfe = 0.1040

Prob = 0.0022







# Match Data

